JOURNAL OF MATERIALS SCIENCE **33** (1998) 5455–5462

A study of the mechanical properties of highly porous ceramics using acoustic emission

J. AUÉ, J. TH. M. DE HOSSON*
Department of Applied Physics, Materials Science Centre, University of Groningen, Nijenborgh 4, 9747 AG Groningen, The Netherlands
E-mail: hossonj@phys.rug.nl

In this paper the results of indirect tensile tests on highly porous ceramics are presented. A relation between the mechanical strength of the highly porous ceramic materials and Acoustic Emission (AE) has been established. We have shown that the amplitude distribution of the AE events depends on the crack velocity, which itself depends on the stress intensity of the crack. Apart from the Brazilian (side crushing strength) tests also multi-point loading experiments were carried out. The AE results show the additional damage accumulation due to compressive/shear stresses.

1. Introduction

This paper concentrates on the mechanical properties of highly porous ceramics, in which microstructural features are the most determining factor. These highly porous ceramics can be regarded as a geometrically random skeleton. Recently random [1–3] and porous [4] materials received increasingly international scientific attention due to their interesting properties in the framework of crack nucleation, propagation, failure and scaling behaviour.

The highly porous ceramics under investigation are used in the chemical industry as catalyst carriers. Its large (internal) area per volume, creates a very large specific area and this high inner surface area (typical 250 m^2/g) provides a large contact area between catalyst and the material being converted. Porosity in these materials may easily attain up to 70 vol % and pore diameters in these materials are usually between 7 nm and 200 nm, which can be fine-tuned using particular processing. Decreasing the pore size of these materials will increase the specific area, but may also lead to a conditional reaction, since the material may act as an molecular sieve. These properties only reflect the chemical aspects of the material, but there are also motivations to study these materials, that stem from a materials science point of view. Indeed, these materials must be able to operate in typical petro-chemical conditions and must therefore have suitable mechanical properties in order to withstand the applied load under operation. These materials are typically used in chemical reactors. Problems will arise when catalyst carriers at the bottom of the reactor crumble under the load of other carriers. The flow through the reactor is affected by this and efficiency of the process will diminish. Thus the mechanical properties are of great importance to the practical performance of the carrier.

For our experiment, two different series of materials have been made, one based on the silicate technology, the other based on the alumina technology. The essential differences among the series are found in the processing parameters, i.e. the mixing times and the types of additives added during mixing. Using these processing parameters, the pore-structure of the material can be determined very accurately. These processing parameters do however also affect the extrusion-behaviour which on its turn will affect the mechanical strength of the material, due to the fact that different amounts of compaction are experienced during the extrusion.

In order to characterise the mutual differences in strength between different batches of porous ceramics, the batches were tested on their ultimate tensile strength. The actual mechanical test we used is an indirect tensile test, which we call the side crushing strength (SCS) test. In this test, a cylindrical shaped specimen is uniaxially deformed at a constant strain rate until it fails [5]. The principal stress under these conditions is a tensile stress perpendicular to the direction of deformation, as has been shown in Fig. 1. The test is actually developed for use on thin discs, where a plane stress situation can be achieved. We do however assume that the contacts between the test plate and sample can be approached by line contacts, which is not always the case. For optimal results the specimen have to be as straight as possible. If we assume the specimen to be a perfect cylinder, the stress at failure can be calculated using the following equation:

$$\sigma = \frac{2F}{\pi L D} \tag{1}$$

In this equation F is the force at failure, L the length of the specimen and D its diameter. In the experiments

* Author to whom all correspondence should be addressed.

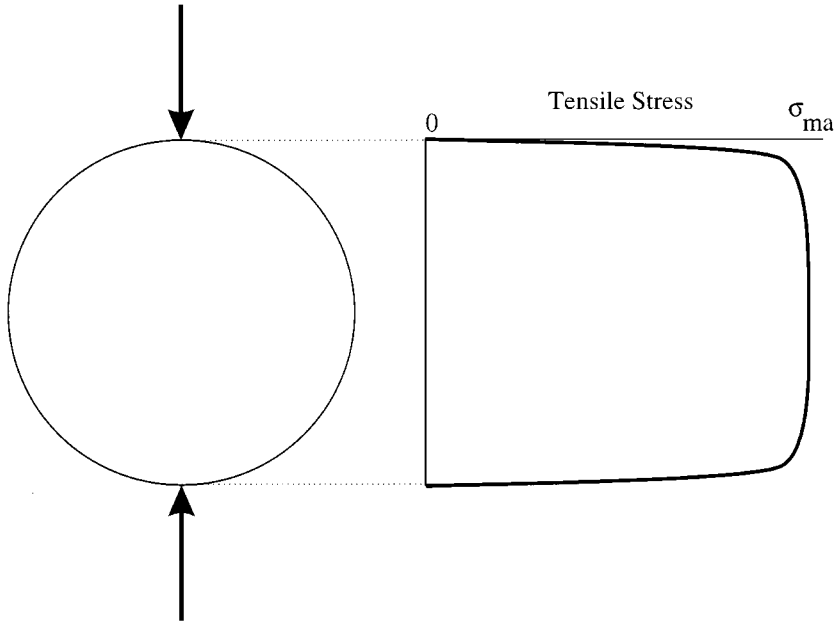

Figure 1 The side crushing strength (SCS) test and its tensile stress distribution in-between the points of contact.

the majority (>80%) of the specimen broke in two half cylinders, in-between the line contacts, suggesting that fracture indeed initiates under tensile stress. The test protocol demands that the test is stopped if the force drops to 60% of the maximum force measured. This maximum force is defined as the force at failure. The test is skipped when fracture patterns other than those expected to come from failure under tensile stress are observed. A typical test involves testing between 50 and 100 specimen of the sample.

Since these disordered materials are brittle in nature, fluctuations in the mechanical strength are to be expected. Actually, the failure strength does not only depend on the microstructural features, but also on the macroscopic size of the specimen. So, instead of investigating the average strength, we describe the mechanical strength by a complete failure distribution. Often the empirical Weibull distribution is used, but more recently, Duxbury and Leath (D-L) proposed another type of failure distribution [6]. The principal difference with the Weibull statistics is that here a different volume dependence is introduced by considering explicitly a distribution function of the size of the cracks. While the Weibull approach is based on the weakest link principle, that is to say the chance on a larger crack scales with the volume, D-L's model implies a 'hottest spot' criterion where failure occurs at the site of the largest local stress. Duxbury and Leath used a defect size distribution, defects being the prime reason for stress concentration, and derived a failure distribution for lattice models:

$$F_V = 1 - \exp\left[-cV \exp\left(\frac{-k}{\sigma^{\mu}}\right)\right] \qquad (2)$$

The Duxbury-Leath distribution is found to describe the weaker specimen better [7] than the Weibull distribution does. Both distributions, the Weibull and D-L, assume that global failure occurs when fracture is initiated. However, this would only be the case for ideal brittle materials and in practice we see damage being built up before global failure occurs. The strength of a batch of material can be characterised by the expectation value, $\sigma_{1/2}$, which is the stress at which a specimen of standardised volume (so we can compare results of different batches) has a 50% chance on failure.

2. Experimental

2.1. Sample preparation and characterisation

The samples investigated were made either of Al_2O_3 or amorphous SiO_2. The initial powders were commercially manufactured by precipitation in stabilised solutions. Subsequently, this precipitated solution is spray dried into powder particles with a typical size of 50 μm. From these powders a slurry is produced which is extruded using a screw extruder. The shape of the extrudates can be varied using different dies. Most materials were extruded as cylinders. The resulting extrudates were dried and subsequently sintered at different temperatures but typical at a temperature of 650 °C. The mechanical properties are strongly dependent on the sintering conditions and extrusion pressure.

In total fifteen batches of material are investigated. The first 5 batches (A . . . E) are all of SiO_2 powder and so is batch O. Differences can be found in slight changes of recipe and processing. The next 5 batches (F . . . J) and batch P are made of Al_2O_3. In all these batches, slight changes in recipe have been made, affecting microstructural features as well as mechanical properties.

The extrudate samples were prepared with greatest care in order to guarantee extrudates as straight as possible. Bent samples will cause bending moments during the tests (especially in the case of more point testing) whereas in the ideal case we only have pure tensile stresses. Before being dried, all extrudates were put into a stainless steel mould were they could be cut at equal lengths of about 10 mm.

The pore size distribution was measured using mercury porosimetry. Using this technique one can

determine the pore-size distribution from the pressure-intrusion curve of mercury, assuming a certain type of pore shape and measuring effectively the most narrow necking.

2.2. Mechanical testing

The testing was performed on a Hounsville 5000E tensile testing machine, equipped with either a 500 N load-cell or a 5000 N load-cell, at a cross-head speed of 0.5 mm/min. This testing machine is completely computer controlled. The load is constantly sampled and when the force drops to 60% of the maximum force up till then, the test is stopped. Because moisture affects the strength of the extrudates negatively, the specimen are dried for 3 hours at 150 °C before testing. During testing, the specimen to be tested are heated above 100 °C until the moment they are placed in the tensile testing machine.

2.3. Acoustic emission

The acoustic emission equipment used was a Physical Acoustics LOCAN 320. The acoustic transducers were of the resonant type (with a frequency range of 100–300 kHz) and were mounted on a specially developed anvil (Fig. 2) in order to avoid unwanted reflections of the acoustic signals. Silicon vacuum grease was used as a coupling agent and the pressure with which the transducers were mounted, using a pressure rig (Fig. 2C), has been standardised [8] in order to keep the sensitivity constant.

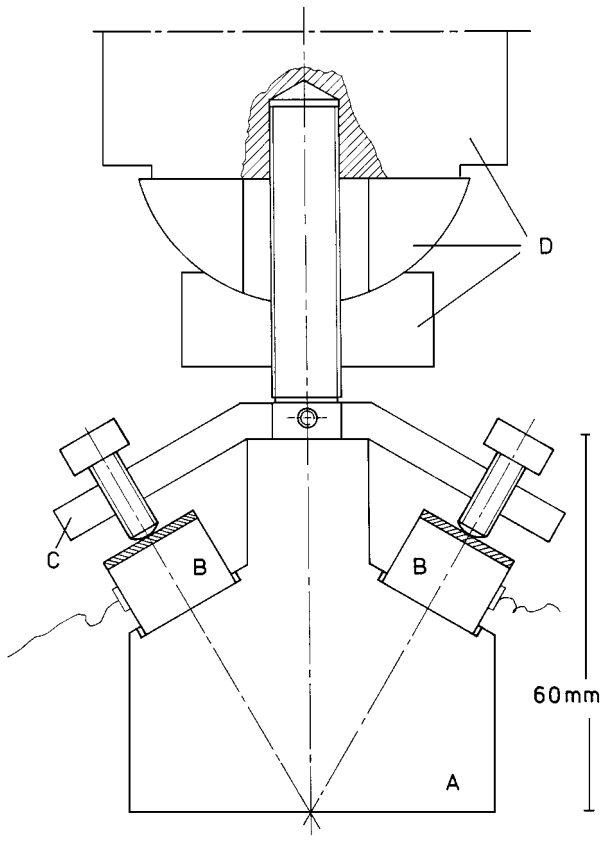

Figure 2 The anvil as used in our crushing experiments. Part A is used to crush the specimen, B are the acoustic transducers and C is the pressure rig used to mount them. Part D is used to align the anvil.

The LOCAN 320 equipment does not sample the whole acoustic pulse but it characterises an acoustic event in terms of amplitude, duration, counts, rise-time and energy. Because we use a resonant piezo transducer, one has to be careful with interpreting the acoustic data. For example, frequency and damping of the signal are real piezo properties and not properties of the incoming signal itself. Only the (maximum) amplitude of the signal will be correlated to the acoustic event itself (mainly to the energy released in the event). This is why we will only look at the distribution of acoustic amplitudes [9].

Two resonant transducers were used during all tests in order to keep the set-up symmetrical. Before each test the sensitivity of the set-up and the mutual differences between the transducers were tested using the standardised ASTM “pencil-break [10]” test. The use of two sensors enabled us to check for acoustic noise. Only if an event was recorded more or less simultaneously on both transducers, it was accepted.

The maximum amplitude that can be sampled using this equipment is 100 dB. All signals with peak amplitudes higher than 100 dB will consequently be recorded as 100 dB peaks. The analysing software of the Locan 320 measurement program offer some on-line filtering settings, which mainly deals with the systems timing. The threshold controls the sensitivity of the system and it represents a level which the signal has to exceed in order to be registered. The peak definition time is used to determine the peak amplitude of the acoustic event. It is re-triggered with each (local) maximum of the signal and if no new maximum is measured within this time window, this maximum is considered to be the maximum amplitude of the acoustic event. The hit definition time is the time window that is re-triggered with each threshold crossing. If the threshold is crossed again within this time window, the system concludes that this part of the signal should be added to the event. If a threshold crossing occurs outside this time window, it is considered to be another acoustic event. The hit lockout time shuts the sensors down for a specific time in order to filter out as much reflections of the signal as possible.

The settings we have used are the following:

Fixed threshold: 45 dB.
Peak definition time: 20 μs.
Hit definition time: 50 μs.
Hit lockout time: 300 μs.

We also sampled the voltage signal of the load cell together with the acoustic emission data. So, for each acoustic event the actual load at that particular moment was recorded. Experimentally we have observed that global failure of a sample always is accompanied by a high energetic acoustic event with a recorded peak amplitude of 100 dB. This enabled us to determine the exact force at the moment of global failure, which showed to be considerably lower than the forces as measured by the standard method. Especially in the case of mixed tensile and compressive stress, considerable differences between these values were found. After global failure has occurred, a lot of acoustic activity was witnessed, probably due to frictional AE sources. In order to filter

these events, all the acoustic events occurring after this 100 dB peak at failure were considered being noise and were not taken into account. Also signals with a number of counts smaller than 10 were removed. Most of the times these very short signals originated from only one of the Piezo transducers. Amplitude and number of counts of these signals did not agree with each other.

2.4. The Gutenberg-Richter relationship

The acoustic emission amplitude distribution is characterised by the so-called Gutenberg-Richter relationship [11], which is well known from earth quake science. In geophysics it is used to predict the chance on an earth quake of a certain magnitude, based on the shocks that had already occurred. This relationship essentially characterises the cumulative amplitude distribution as a power-law shaped function:

$$\log N(W) = a_{\mathrm{GR}} - bW \tag{3}$$

In this simple equation, $N(W)$ is the number of earth quake events of a size greater than or equal to magnitude W, a_{GR} is a constant and b is the seismic b-value. In literature [12] it has been suggested that this widely used empirical relationship also can be applied to acoustic emission data, once a correction factor of 20 is introduced to correct for the fact that AE amplitudes are measured in decibels rather than the logarithmic peak amplitude of the Richter scale. For these AE measurements we call b the AE b-value. The relation can be fitted to both discrete or cumulative amplitude distributions, the latter being used in geophysics. Typical values of this AE b-value are in the range between 0.4 and 2 and the b-value is often associated with the pace of the fracture process. If the deformation proceeds by a small number of large energetic events, there is a relatively large amount of high amplitude events and the b-value is small. On the other hand, if the fracture process proceeds in a large number of small events, the b-value is large.

The exact physical meaning of this AE b-value is somewhat obscure in the geophysical literature at this moment, but a connection with self organised critical systems has been suggested [13]. As will be discussed later in this paper, here we suggest that the AE b-value depends on the dynamics of crack growth in terms of time dependent stress intensity factors and energy release rates.

3. Experimental

As can be seen from Fig. 3, where we have plotted logarithmically the cumulative number of events with a certain amplitude against its amplitude, the AE signal amplitude distribution indeed does show a power-function like behaviour, as described by the Gutenberg-Richter relationship. The most striking result of the AE measurements however is that, as can be seen from Tables I and II, the AE b-value seems to decrease with increasing expectation value $\sigma_{1/2}$. Note that the power-function constant a is corrected for the number of AE tests and the AE b-value, is corrected with a factor of 20 due to the fact that the measured amplitudes are in decibles.

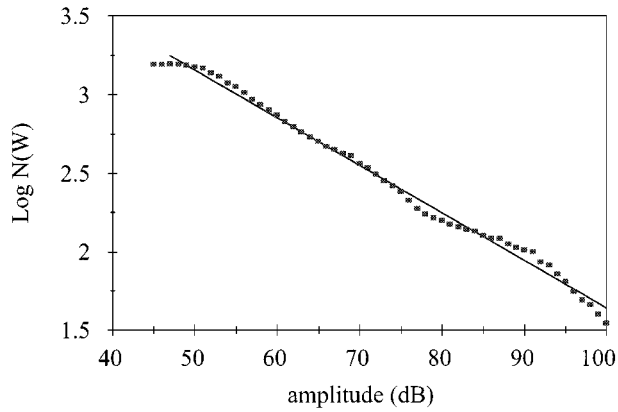

Figure 3 Power function like behaviour of the amplitude distribution, as expected from Gutenberg and Richter.

TABLE I Results of the SCS tests on SiO_2 extrudates. The mechanical properties are characterised using the Duxbury-Leath parameters k and ln c and the expectation value $\sigma_{1/2}$. The AE data is characterised using the AE b-value and the a_{GR} constant

Material	No. of SCS tests	k	Ln c	$\sigma_{1/2}$ (MPa)	AE-b	a_{GR}	Pore size (nm)	Pore vol. (ml/g)
A61	100	15.6	19.6	4.9	0.42	2	18.8	0.95
B62	94	12.5	19.8	3.7	0.38	1.6	18	1.04
C63	101	14.8	20.6	3.6	0.4	1.86	20.1	1.13
D64	100	12.3	20.2	3.3	0.62	2.32	21.4	1.15
E66	84	9.8	19.8	2.9	0.63	3.11	19.1	1.09

TABLE II Results of the SCS tests on Al_2O_3 extrudates. The mechanical properties are characterised using the Duxbury-Leath parameters k and ln c and the expectation value $\sigma_{1/2}$. The AE data is characterised using the AE b-value and the a_{GR} constant

Material	No. of SCS tests	k	Ln c	$\sigma_{1/2}$ (MPa)	AE-b	a_{GR}	Pore size (nm)	Pore vol. (ml/g)
F1	100	46.5	21.2	9.8	0.39	1.82		
G8	100	29.7	19.8	8.9	0.34	1.63	7.6	0.58
H9	100	4.99	17.9	3.4	0.52	2.46	7.5	0.56
1I0	100	26	19.4	8.8	0.37	1.8	7.7	0.6
J703	101	13.5	19.1	5.1	0.47	2.26		

This decrease in the AE b-value with increasing $\sigma_{1/2}$ has been observed for both the silica and the alumina extrudates. There are however some differences in acoustic behaviour between these two different materials. The rate of decline of the AE b-value with increasing $\sigma_{1/2}$ is for the silica extrudates much higher than for the alumina extrudates.

Important for establishing the exact moment and force at global failure is the fact that we observed global failure always to be accompanied with a high amplitude acoustic event (100 dB). Very little acoustic activity unto this moment of failure was observed. Tests stopped directly after measuring this acoustic peak amplitude, showed the specimen to have a fracture plane across the complete sample, from contact point to contact point along the plane of highest tensile stress. Also the load, recorded simultaneously with the acoustic data, showed a local force drop. Sometimes however, the test would continue for a while after a 100 dB peak had been measured. This was caused by the fact that both halves of the specimen would still stick together after fracture and withstand the applied load. Due to the friction of both fracture planes sliding over each other, a lot of frictional AE events were produced (mainly of low amplitudes and a very low number of counts). In order to remove these signals, the acoustic data was filtered, as described in. A side effect of this is that the SCS value as determined using the conventional maximum force readout of the loadcell before a 60% force drop was measured (according to the standard SCS protocol), is found to be about 20% higher than the actual force at failure as witnessed by the AE equipment. Using the standard SCS protocol will thus lead to a systematically overestimate of the tensile failure strength of our samples.

4. Discussion

The most noticeable effect we have observed in these experiments, is the relation between the AE b-value and the failure stress. The variation in the AE-b value implies a change in the amplitude distribution and could point to different failure mechanisms.

In general, the lower strength materials show a high a_{GR} in combination with a high AE b-value, indicating that many (secondary) crack are formed (low amplitude events) prior to global failure. This suggests that damage is steadily being built up and that coalescence of the secondary cracks results in global failure. The stronger materials show much less crack growth (low a_{GR}) and a shift towards the higher amplitude events can be seen, meaning that these materials fail mainly through the growth of primary cracks.

More precisely, it is suggested that a_{GR} is linear proportional to $\log f_\alpha$, where f_α represents the crack density of cracks with a particular length a and a particular orientation α with respect to the applied stress. The reasoning is based on the fact that the change in energy is directly proportional to the crack advance dl. A next step is the assumption that the crack advance depends on the initial crack length a_α^μ. Writing the crack density per unit of area (f_α/a_α^μ) as ρ_α, $\log \rho_\alpha$ vs $\log E$ yields an intercept, i.e. a_{GR}, proportional to $\log f_\alpha$. As a result the a_{GR} factor can be related to the crack density of the material.

The failure behaviour during the SCS test can in general be regarded as a catastrophic event, since in the majority of the tests, little acoustic activity could be measured up till the moment of failure. This would imply that we indeed can use failure distributions which regard failure as a catastrophic event, such as the Weibull weakest link approximation or the Duxbury-Leath "hot spot" approximation.

The dependence of the AE b-value upon the material and its strength can discussed by investigating the relation between the crack velocity in the material and at its energy release rate. From these two materials properties a physical description should emerge that explains the failure stress dependence of the AE b-value. Our starting point will be based on the dynamic aspects of crack growth phenomena, rather than on quasi-static descriptions. We consider the planar crack to grow through an elastic isotropic material under plane strain conditions and the tensile opening mode I is assumed. As the cracks grow, the area in-between them decreases in size whereas the stresses in these gaps increase. As long as the crack velocities are small compared to the elastic wave velocity (Rayleigh wave velocity) c_{R}, the growth can be calculated quasi-statically. However, at some point the rate of disappearance of the stressed regions will grow and the velocity of the crack will approach the sonic speed. It is reasonable to argue that at the beginning of the crack growth in our porous materials, the smallest areas between the cracks will disappear first, with a small release of mechanical energy stored in these areas. At a later stage, fusion between larger cracks or the collapse of large stressed areas, will release a larger amount of energy, i.e. a shift in the energy spectrum which can be described by a lower AE b-value will occur. Consequently, at first sight we take the Gutenberg-Richter exponent b inversely proportional to the crack velocity. A higher velocity leads to a higher energy release that can be described by a lower AE b-value. In literature [14–16] the experimentally determined crack velocity V depends on the stress intensity factor K, according to:

$$V = V_0 \exp\left(\frac{K}{K_0}\right) \tag{4}$$

or

$$V = V_0 \left(\frac{K}{K_0}\right)^n \tag{5}$$

These rather empirical relations, which obviously must be wrong at high K values, can be based on a more fundamental footing. The crack velocity $\dot{a}$ is given by [17]:

$$\frac{\dot{a}}{c_{\mathrm{R}}} = 1 - \frac{EG}{(1-\nu^2)K^2} \tag{6}$$

where the stress intensity factor K is assumed to have little variation over the crack growth distance. If K is

equal to K_{Ic}, the crack quasi-statically starts to move at $\dot{a} = 0$. With increasing stress, K increases and the crack speeds up to higher velocities until the Rayleigh wave velocity of the material is attained. On a macroscopic scale the energy release rate G may be simply connected to a uniform homogeneous resistance force Γ_0 where Γ_0 describes the surface free energy needed to create a free surface. However, at a microscopic scale G is determined by a (non-)periodic resistance depending on the local stress fields, the inhomogeneities, the crack distribution etc. As a result, the energy release rate in Equation 6 will at a microscopic level depend on a function θ of the cracktip position p: $G = \Gamma_m \theta(p)$ where Γ_m is a constant, being the maximum fracture energy. At a microscopic level, the crack velocity will be the averaged speed, determined by the microscopic fracture resistance:

$$\bar{V}(K) = c_R \left[\int_0^1 \left(1 - \frac{E\Gamma_m \theta(q)}{(1-\nu^2)K^2} \right)^{-1} \mathrm{d}q \right]^{-1} \quad (7)$$

Equation 7 follows directly from 6 and on a macroscopic level we may rewrite Equation 6 as:

$$\bar{V}(K) = c_R \left(1 - \frac{E\Gamma_0}{(1-\nu^2)K^2} \right) \quad (8)$$

where Γ_0 is the uniform fracture energy. At high values of K, i.e. high stresses, the uniform crack velocity as in Equation 7 can be approximated by [17]:

$$\bar{V}(K) = c_R \left[1 - \frac{E\Gamma_m}{(1-\nu^2)K^2} \bar{\theta} \right] \quad (9)$$

where it is assumed that $\theta(p)$ is periodic function with $\bar{\theta}$, averaged over a spatial period. The Rayleigh velocities in (pure) Al_2O_3 and SiO_2 as calculated from the elastic moduli and Poisson's ratio's are 5.5 km/s and 3.3 km/s, respectively. Using the appropriate values for the energy release rate and the fracture toughness, the crack velocities for both materials are displayed in Fig. 4.

As already mentioned earlier in this section, higher crack velocities are associated with the fusion between larger cracks or the collapse of large stressed areas, will release a large amount of energy. As the stress intensity factor K is linearly proportional to σ, $|b|$ is expected to decrease with increasing $\sigma_{1/2}^{-2}$. This decrease is indeed observed experimentally, as can be seen in Fig. 5.

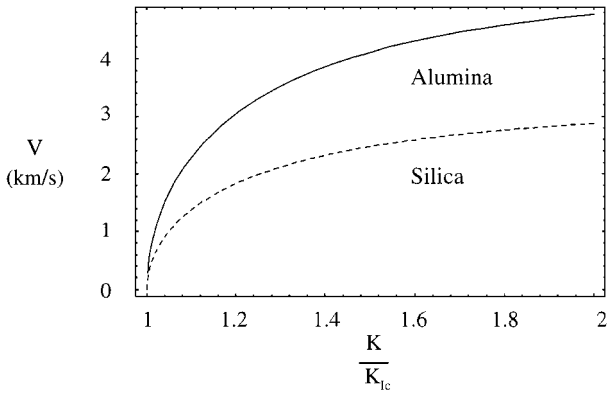

Figure 4 The crack velocity as a function of the applied stress level.

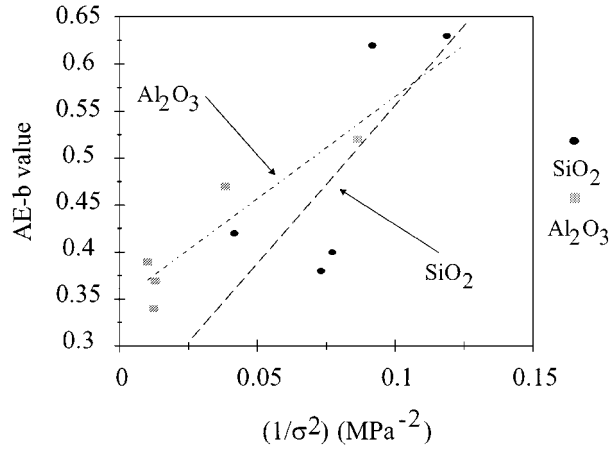

Figure 5 The AE b-value for SCS test on SiO_2 and Al_2O_3 extrudates as a function of $\sigma_{1/2}$.

In principle the amount of energy radiated out of the fracture process E_R can be formulated, since it is equal to the difference between the apparent energy flow into the crack tip (Γ_0) and the actual energy consumed ($\Gamma_m \bar{\theta}$). However the amount of radiation energy measured in AE experimentally is much smaller than E_R, due to scattering and absorption of the radiated signals. For that reason a detailed comparison between theory and experiment is not appropriate.

An interesting point for discussion is whether acoustic emission and the accompanied analysis based on the Gutenberg-Richter relationship may detect differences between tensile and compressive stress fields. Therefore, apart from the Brazilian (SCS) test, also multi-point loading conditions were considered. This is not the first time that different loading conditions are compared. For example, Vardar and Finnie [18] related the results of three point bending tests to the Brazilian Test, discovering limitations of the Weibull treatment in multi-axial loading conditions. We have carried out additional experiments, where not only tensile stresses are present, but compressive stresses are introduced by having more than 2 line contacts (Fig. 6). The contribution of compressive stresses can be controlled by varying the angle between the different contacts. The goals of these experiments are to investigate the effects

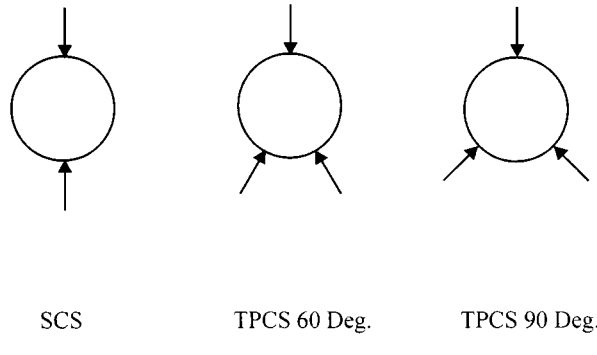

Figure 6 Multiple point tests: the side crushing strength (SCS) test and two three-point crushing tests (TPCS).

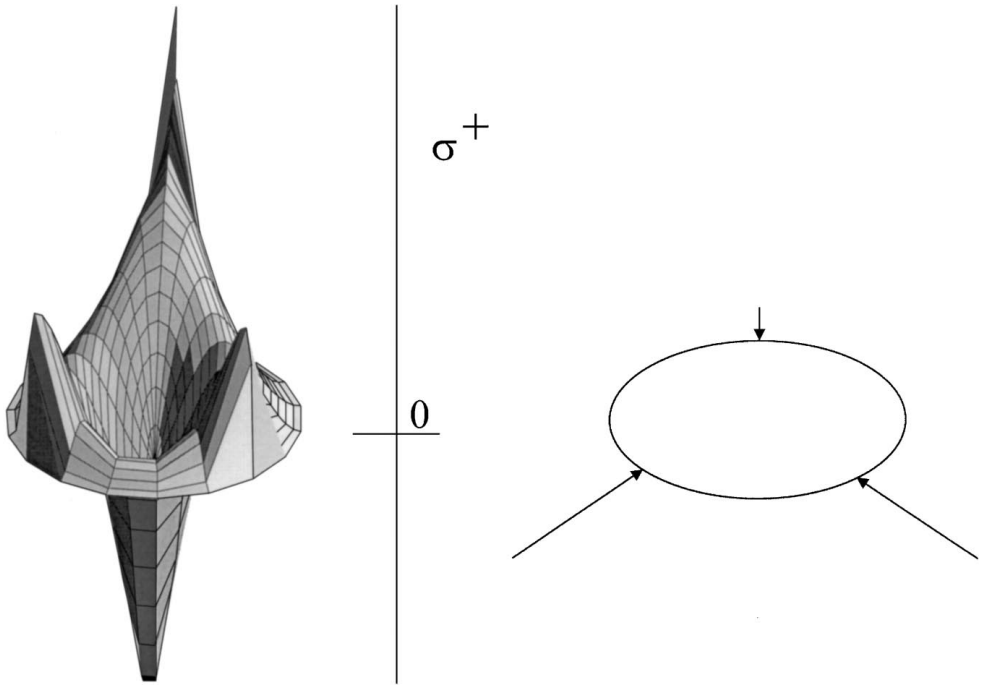

Figure 7 Calculated (radial) stress distribution, in arbitrary units, of a TPCS 90° test. The figure shows a cross-section of the actual sample.

of compressive stresses on the acoustic emission can be studied and to see to what extent the compressive stresses play a role in the fracture processes. In the experiment with a moderate amount of compressive stress the line contacts had an angle of 60° with respect to each other. Higher compressive stresses could be reached using an angle of 90° between line contacts (Fig. 6). The calculated stress distribution in the case of a TPCS 90° test is figured in Fig. 7. Especially in the multiple-point testing case, much attention was paid to the alignment of the anvils with respect to each other. The anvils were adjusted with a misalignment of less than 1 in 1000. The results of the multiple-point tests are summarised in Table III. As can be seen, the absolute (average) force at failure indeed increases if we increase the externally applied compressive stress. The mean force as displayed in the table is corrected for the average length of the extrudates and expressed in N/cm. One should also note that these mean forces are taken from the acoustic measurements according to the procedure as discussed in Section 2.

TABLE III Results of the multiple point tests. The absolute force at failure is expressed in N/cm and the AE data is characterised using the AE b-value

Material	Test	$\langle F \rangle$ N/cm	AE b-value	a_{GR}	Ratio to SCS
O65	SCS	104	0.61	3.03	—
	TPCS 60	134	0.8	4.03	1.29
	TPCS 90	128	0.84	4.32	1.23
E66	SCS	124	0.63	3.1	—
	TPCS 60	124	0.87	4.22	1
	TPCS 90	118	0.87	4.31	0.95
J703	SCS	228	0.47	2.26	—
	TPCS 60	345	0.66	3.31	1.51
	TPCS 90	347	0.73	3.65	1.52
P713	SCS	144	0.68	3.41	—
	TPCS 60	210	0.76	3.91	1.46
	TPCS 90	205	0.8	4.14	1.42

The stopping criterion of a force drop to 60% of the peak force had to be changed to at least 90%, since the presence of compressive stresses made the force drop after failure much smaller. If the test was not stopped on time, much AE noise was generated. We also observed saturation effects of the AE measurements at high emission rates and especially at high amplitudes. This is likely to be caused by coincidence [19] of pulses. If two pulses arrive within the Hit Definition Time (HDT) at the same transducer, they will be seen as one pulse. The duration of both pulses will consequently be added and the highest amplitude of the two will granted to the composed pulse. Especially at higher emission rates this can be a problem, since duration, number of hits and amplitude do not agree with each other anymore, giving another argument for only using the amplitude of the acoustic event as a measure for its energy (instead of the often used "ring down" approach). This saturation effect will presumably cause that a number of high energy AE signals is not being measured.

During the multi-point deformation tests, much more acoustic activity before the moment of failure was witnessed than in the SCS case. Also an increase in the a_{GR} could be witnessed when going from the SCS to TPCS 60° and to the TPCS 90° test. The increase of the AE b-values that accompanies this, suggests that a lot more low energy events occur, what can be associated with damage accumulation. This suggests that the compressive stresses that have been applied, indeed play a role in these kind of loading conditions and cannot be neglected. This also leads to a situation where failure cannot be regarded as a purely brittle event, where failure occurs through (rapid) propagation of primary cracks, and deviation from Weibull statistics is to be expected.

The Weibull model also does not incorporate the possible influence of a compressive/shear stress field, since it can only be applied to tensile failure. The failure stresses from the experiments with highest compressive/shear stresses are lower than predicted based on a pure Weibull model. This makes it most probable that the induced shear stress component of the stress field does play an active role and cracks initiated under Mode II and III conditions are of influence on the failure behaviour.

5. Conclusions

In this paper we have discussed the testing of mechanical properties in relation to acoustic emission. We have used acoustic emission successfully, enabling us to characterise the failure characteristics during deformation of highly porous ceramics and to pin point the exact moment of failure. The amplitude distribution of the acoustic signals showed to scale as a power-function, according to the Gutenberg-Richter relationship. This scaling can be characterised using the AE b-value, which can be expressed in terms of materials constants and seems to depend on the energy release rate of the material involved. We have observed the AE b-value to decrease with increasing strength. The rate of decline of this acoustic b-value is much larger for silica extrudates than for alumina extrudates. We have suggested that the AE b-value is related to the crack velocity, which itself depends on the actual stress intensity of the crack. As the higher crack velocities are associated with the collapse of large stressed areas, increasing crack velocities will lead to a decreasing AE b-value. The a_{GR} constant can directly be associated with the (logarithmic) crack density of the material. In the case of pure tensile stresses, failure has been observed to be a catastrophic event. Only in the case of weak samples some accumulating damage could be witnessed. When compressive/shear stresses are involved, failure exhibits a different character. We see damage accumulation to occur in both alumina and silica extrudates and we see this probably shear stress induced damage accumulation to play an active role in the failure mechanism of the specimen.

References

1. J. C. CHARMET, S. ROUX and E. GUYON, "Disorder and Fracture" (Plenum Press, 1990).
2. S. ROUX, "Probabilities and Materials" (Kluwer Press, 1994) 163–75.
3. E. GUYON, S. ROUX, A. HANSEN, D. BIDEAU, J. P. TROADEC and H. CRAPO, *Reports on Progress in Physics* **53**(4) (1990) 374–419.
4. L. J. GIBSON and M. F. ASHBY, "Cellular Solids: Structure and Properties" (Pergamon, 1988).
5. P. J. F. WRIGHT, *Magazine of Concrete Research*, July (1955) 87.
6. P. M. DUXBURY and P. T. LEATH, *J. Physics A* **20** (1987) L411.
7. I. C. VAN DEN BORN, Mechanical strength of highly porous ceramics, Ph.D. thesis University of Groningen, 1992.
   I. C. VAN DEN BORN, A. SANTEN, H. D. HOEKSTRA and J. TH. M. DE HOSSON, *Phys. Rev. B* **43** (1991) 3794.
8. Y. HIGO and H. INABA, The general problems of AE sensors, Acoustic emission: current practice and furture directions, ASTM STP 1077.
9. A. A. POLLOCK, Non destructive testing, October (1973) 264.
10. ASTM Designation E976-84, "Standard Guide for Determining the Reproducability of Acoustic Emission Sensor Response," Philadelphia, 1984.
11. B. GUTENBERG and C.F. RICHTER, *Bull. Seismol. Soc. Am.* **32** (1942) 163.
12. C. G. HATTON, I. G. MAIN and P. G. MEREDITH, *J. Struct. Geol.* **15** (1993) 12, 1485.
13. P. DIODATI, F. MARCHESONI and S. PIAZZA, *Phys. Rev. Lett.* **17** (1991) 67, 2239.
14. J.K. ATKINSON, *J. Geophys. Res.* **89** (1984) 4077.
15. T. YAMASHITA and L. KNOPOFF, *Geophys. J. Roy. Astr. Soc.* **96** (1989) 14.
16. L. KNOPOFF, in "Disorder and Fracture," edited by J. C. Charmet, S. Roux and E. Guyon (Plenum Press, New York, 1990) p. 289.
17. L.B. FREUND, "Dynamic Fracture Mechanics" (Cambridge University Press, 1993).
18. O. VARDAR and I. FINNIE, *Int. J. Fracture* **11** (1975) 495.
19. E. U. OKOROAFOR and R. HILL, *J. Mater. Sci.* **30** (1995) 4233.

Received 25 March 1997
and accepted 18 September 1998